In situ characterization of deformation behavior of austenitic high manganese steels

Sascha Hoffmann*, Wolfgang Bleck, Banu Berme

RWTH Aachen University, Department of Ferrous Metallurgy, Aachen, Germany
hoffmann@iehk.rwth-aachen.de

Keywords: TWIP, TRIP, serrated flow, mechanical testing

Abstract: The mechanical properties of high manganese steels are linked to their hardening mechanisms and their intrinsic behavior during deformation. The characterization of mechanical properties is influenced by the localization of plastic flow and the effect of this localization on the material. Depending on grain size, temperature and extrinsic strain rate localization of strain, adiabatic heating and hardening vary in spatial and temporal extent. Even at small strain rates the adiabatic heating of samples reaches temperatures more than 100K over initial testing temperature due to the sharp localization and last but not least this heating is also dependent on the tested sample size. Furthermore temperature influences the activated mechanisms of plastic flow. The characterization of temperature increase, strain distribution and local hardening is pursued in tensile tests with application of infrared thermography. With those techniques it is possible to gather correlations between local strain and temperatures. The analysis of dynamic strain ageing effects is also carried out by evaluation of the instantaneous strain rate, the strain rate in the gauge length, in dependence of stress in different alloys as well as at different strain rate regimes. Thus it is possible to distinguish the onset of TRIP, TWIP and DSA.

Introduction: High manganese steels exhibit excellent mechanical properties in regard to elongation and strength. The exceptional properties are based on Transformation Induced Plasticity (TRIP) and Twinning Induced Plasticity (TWIP) that can be observed in high-manganese steels (HMS). The TRIP-Effect is characterized by the transformation of the metastable austenitic matrix into either hcp or bcc-martensite under mechanical load, in TWIP steels twins are formed during deformation. The stacking fault energy (SFE) was identified as the parameter that controls the activation of these mechanisms [1], [2], [3] and it was found it can be influenced by the chemical composition (mainly Mn and C), as well by change of temperature [2], [3], [4].

The Collaborative Research Centre (SFB761) “Stahl – ab initio” of the Deutsche Forschungsgemeinschaft (DFG) tries to build up fundamental knowledge on the behavior of these new steels by application of advanced modeling techniques, the laboratory scale processing of selected alloying compositions and the characterization of properties of the finished product as cold rolled sheet.

In this evaluation four alloys produced in the frame of collaborative research center (SFB 761) are evaluated concerning their mechanical properties, their hardening behavior and their inhomogeneous flow behavior. Alloy II resembles the most thoroughly examined composition 22Mn0.6C that was also evaluated by Allain in 2002 [5] resp. Allain et al. in 2004 and 2008 [3], [6]. The composition of Alloy VI is similar to the composition examined by Chen et al. in 2007 with 18Mn0.6C [7]. The other two compositions were chosen based on the calculations of SFE of Saeed-Akbari et al. [2] based on thermodynamical modeling of the SFE variations with chemical composition. Alloy I exhibits a similar SFE to Alloy IV but with reduced carbon and increased manganese content. Alloy VII exhibits an even higher SFE than the Allain composition (Alloy II) by increase of carbon content. Aim of this work is to show the influence of chemical composition on mechanical properties, hardening behavior and on the occurrence

of serrated flow. The criteria normally used to evaluate mechanical properties are validated based on the results of the mechanical testing.

State of the Art: The dependency of the mechanical properties from the chemical composition was investigated for a huge variety of high manganese steels in recent years. A huge number of recent works focus on the DSA (dynamic strain ageing) and the propagation of PLC-bands in the tensile specimen during deformation.

In 2007 Chen et al. [7] evaluated the PLC effect of an 18Mn0.6C austenitic TWIP-steel. They could show that deformation of this steel is based on the initiation and propagation of successive PLC-bands which results in a serrated flow curve. The temperature distribution was monitored and correlated with the passage of the bands. Additionally the geometry and propagation speeds of the deformation band were measured. It was found that geometry of bands did not change but speed decreases with increase of strain.

The austenitic steel 22Mn0.6C and its dynamic strain ageing behavior was evaluated by Allain et al. in 2008 [6]. This examination showed the direct correlation of serrations in the flow curve, strain localization and localized heating of tensile specimen. The temperature increase was monitored and correlated with the narrow PLC-Bands. A heating with a ΔT of 20K at fracture was found.

Extensive works on the nature of PLC-Effect in another high manganese steel, in this case a 17Mn0.6C steel, was published by Zavattieri et al. in 2009 [8]. Zavattieri proposed a progressive reduction of sample width during the passage of a deformation band in the gauge length. In addition it was measured that strain rates show huge inhomogeneity during the deformation and passage of a local deformation band when calculated for a very small length using digital image correlation.

Another investigation on steel with similar composition but with addition of aluminum was published in 2009 by Kim et al.[9] In this work the strain rate sensitivity was calculated and its influence on the formation of strain localization in PLC-Band was pointed out.

Experimental Procedures: All investigated steels are available as cold rolled sheet manufactured from 4 laboratory melts with variations in carbon and manganese content. Each melt is done in a vacuum induction furnace and cast in 100kg blocks. The chemical compositions are given in Table 1. After casting the blocks are reheated, forged and annealed for homogenization. The block is cut and hot rolled to 3 mm thickness followed by a cold rolling step down to around 1.5 mm.

Table 1: Chemical composition of the laboratory melts in mass-%.

Alloy	C	Si	Mn	P	S	Cr	Mo	Ni	Main deformation mechanism
I	0,315	0,066	22,79	0,0073	0,0012	0,0016	0,014	0,037	TRIP
II	0,573	0,174	23,21	0,009	0,0002	0,31	0,019	0,0381	TWIP
IV	0,594	0,103	18,4	0,0084	0,0005	0,016	0,02	0,037	TWIP
VII	0,714	0,059	23,5	0,0071	0,0071	0,016	0,01	0,039	TWIP

The specimen geometry is chosen based on the limited amount of rolled sheet and the expected mechanical properties. The geometry is based on a specimen for dynamic tests with broader head and longer gage length. Specimen are cut from the full hard, cold rolled sheet using water jet cutting and are fully recrystallized in a salt bath furnace at 800 °C for 30min. (Fig. 1). Tensile tests at ambient temperature are performed at strain rates of 0.003, 0.03 and $0.1s^{-1}$ using a Zwick Z100 tensile test machine equipped with a videoextensometer for contactless strain measurement.

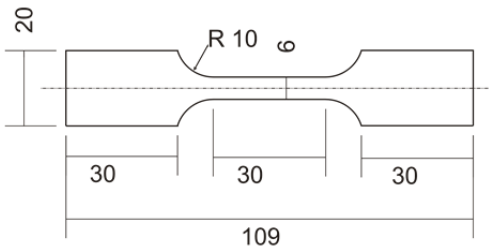

Figure 1: Specimen geometry for quasistatic tensile tests used in this work. All measures are given in mm.

The hardening behavior is evaluated; smoothened hardening curves are used to describe the global hardening behavior. The so called instantaneous strain rate (ISR, Eq. 1), which is the strain rate in the gauge length of the sample, is calculated as the derivative of true strain over time and is plotted versus the true stress based on the work of Akbari [10].

$$\frac{d\varepsilon_w}{dt} = ISR \tag{1}$$

To characterize the localization of plastic deformation the adiabatic heating of the specimen is monitored with an infrared camera infratec pir uc 180. The works of Zavatierri and Chen show that localized temperature increase and localized strain are closely related.

Results and Discussion: The tested laboratory melts show excellent mechanical properties. The tensile properties for the three strain rates are given in Table 2. Tests are performed

Table 2: Mechanical properties transversal to rolling direction at three different strain rates.

Strain rate	Steel	YS (MPa)	UTS (MPa)	UE (%)	TE (%)	n-Value
0.003 s^{-1}	Alloy I	284	825	39.2	40.0	0.46
	Alloy II	312	932	64.9	69.8	0.50
	Alloy IV	335	975	53.1	57.7	0.50
	Alloy VII	315	935	76.1	79.7	0.51
0.03 s^{-1}	Alloy I	307	833	43.3	46.8	0.45
	Alloy II	323	911	59.2	65.1	0.48
	Alloy IV	343	946	60.1	62	0.46
	Alloy VII	325	881	62.5	66	0.48
0.1 s^{-1}	Alloy I	310	817	44.4	48	0.44
	Alloy II	361	849	53	55.3	0.42
	Alloy IV	342	916	58.3	62.1	0.46
	Alloy VII	331	866	60.9	60.9	0.46

All steels exhibit a yield stress around 300 MPa and depending on chemical composition achieve ultimate tensile stresses up to 975 MPa with tensile elongations up to 79.7 %. The yield stresses increase with increasing strain rate while the ultimate tensile stresses decrease. The true stress – true strain curves (Figure 2) show serrated flow behavior for three of the grades (II, IV and VII) in the TWIP-range and a smooth stress strain curve for the TRIP material I. Despite the fact that the SFE of Alloy I and IV is calculated as nearly equal the TRIP alloy I shows no serrated flow while alloy IV shows not only serrated flow but also higher strength at moderately reduced strain. The behavior is similar to the calculated TWIP compositions II and VII.

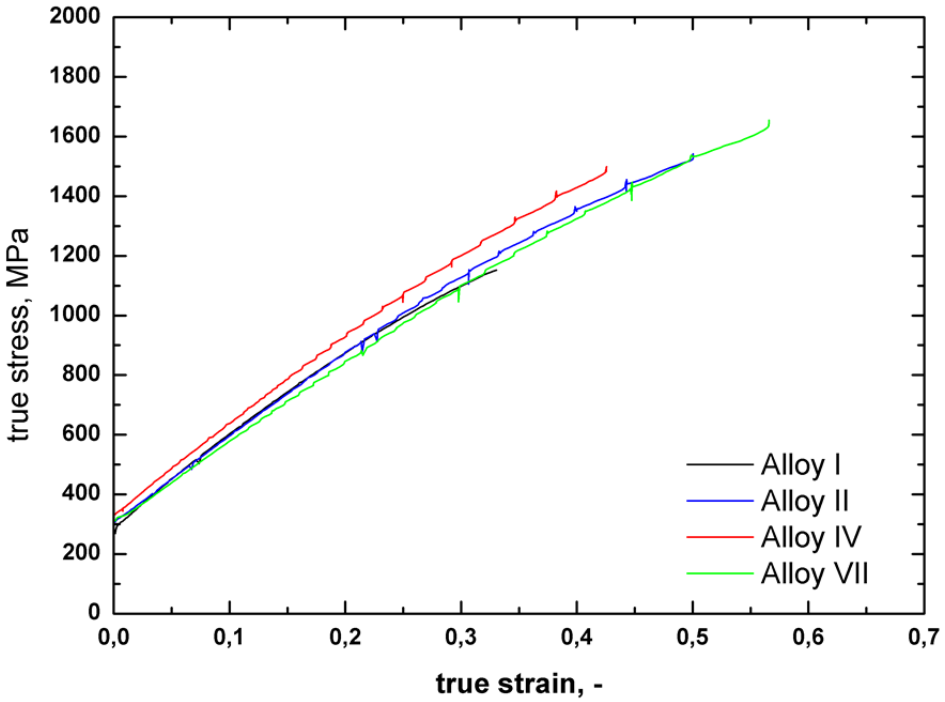

Figure 2: True stress - true strain curves of the four alloys, transversal direction, $\dot{\varepsilon} = 0.003\ s^{-1}$.

The hardening curve is calculated as the derivative of the flow curve. Due to the serrations of the curves the derivative exhibits huge amplitudes of hardening. These do not necessarily describe the overall trend of hardening of the curve, but only the, very localized, stress overload necessary to start the deformation band propagation. Nevertheless each overload is followed by a heavy drop of hardening after a deformation band formed (Fig. 3). This drop can be so severe that for a very short moment the Considère-Criterion for local necking (Eq. 2) is fulfilled.

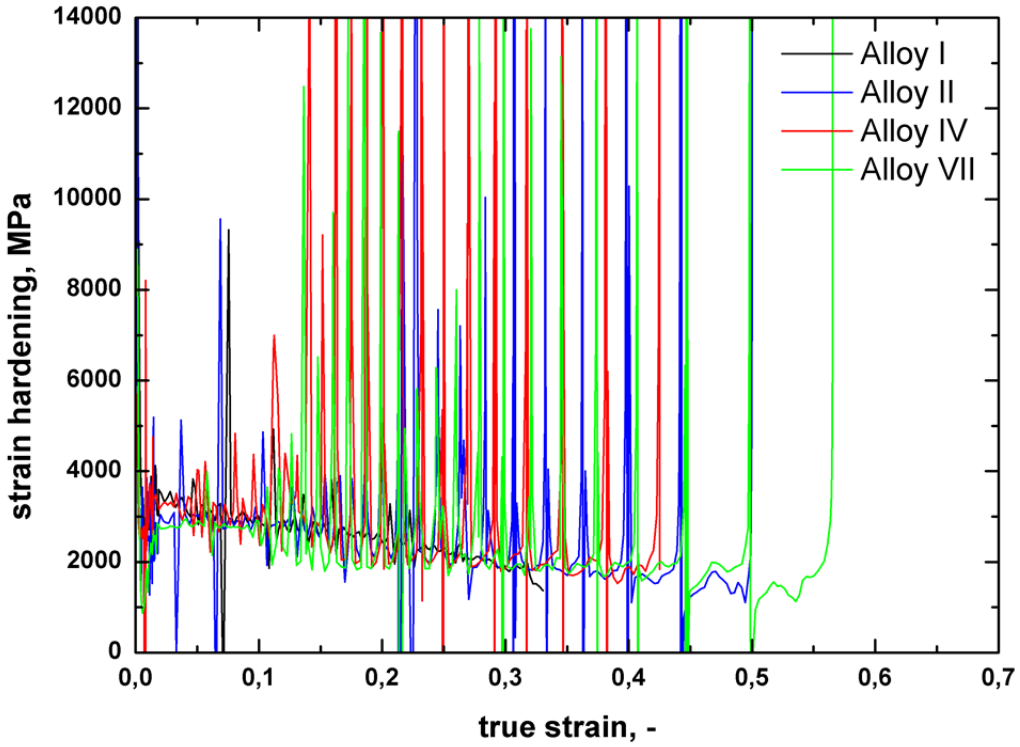

Figure 3: Strain hardening curves for the four alloys, transversal direction, $\dot{\boldsymbol{\varepsilon}} = \mathbf{0.003}\ \boldsymbol{s^{-1}}$.

$$\frac{d\sigma_w}{d\varepsilon_w} = \sigma_w \qquad (2)$$

The local hardening potential stops the further necking and the propagation of the deformation band starts in direction of material with lower hardening state as proposed by Zavattieri. The formation and movement of the bands usually starts in the regions of the sample heads where stress is geometrically concentrated as proposed by Wijler et al. [11]. Neglecting the local phenomena by smoothening of the hardening curve the global hardening in the gage length can be described. It shows very similar hardening behavior for the alloys II, IV and VI due to their twinning behavior. Alloy VII shows the lowest initial hardening. Alloy I shows higher initial hardening but a higher decrease over strain due to the martensite formation during deformation (Fig. 4).

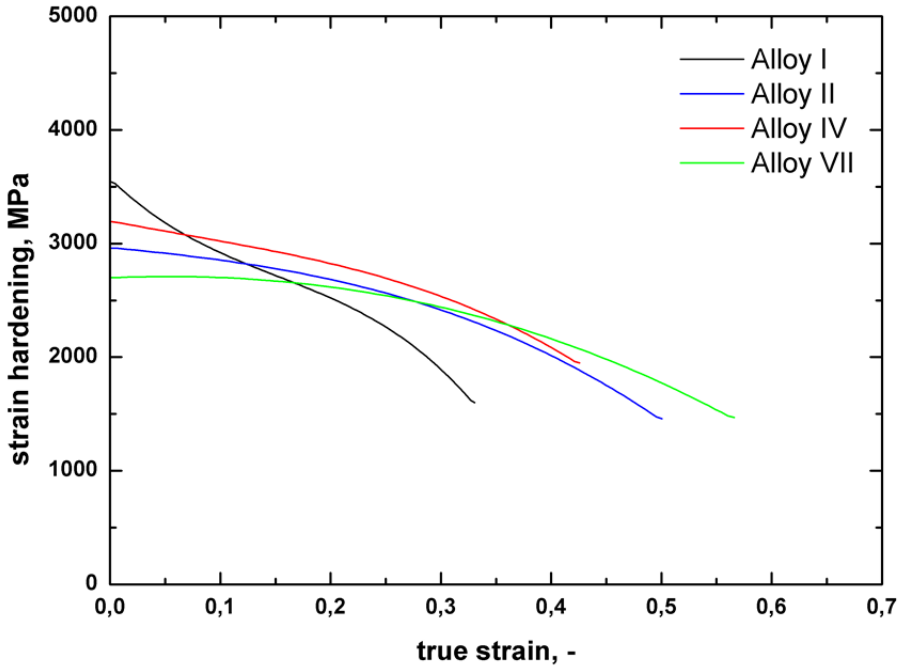

Figure 4: Smoothened strain hardening curves of the evaluated alloys.

Correlated with the localized deformation a localized heating takes place, which leads to a temperature increase of up to 10K for tests on alloy VII at ambient temperature with a strain rate of $0.003s^{-1}$. Increase of strain rate also increases local heating to 35K at $0.03s^{-1}$ and 51K at $0.1s^{-1}$ in this alloy respectively. The TWIP-materials (II, IV and VII) show higher temperatures in the end due to their higher strains. This rise in overall temperature is seen to be the main influence on the decrease in UTS with increased strain rate. The assumption, valid for mild steels, that temperature is constant during a tensile test cannot be applied on HMnS even at small sample sizes with good cooling by heat transfer to the clamps. As SFE is also influenced by temperature it can be proposed that also SFE and by that the deformation mechanisms are not constant during the test. Results from larger specimen (A_{50}) show even higher local heating with even more influence on the SFE. It was also observed during thermography that directly ahead of fracture two deformation bands with opposite directions of propagation met at the crack site.

The strong localization of deformation in the propagating bands leads to a rather unusual strain rate distribution. The so called instantaneous strain rate can be calculated as the derivative of true strain vs. time. The true strain is measured in the gauge length. The propagating deformation bands start moving outside of the gage length and deliver the main contribution to plastic deformation on their passage of the gauge length. The strain rate in the gauge length jumps from a high level while the band passes the gauge length to a low level

while the band moves outside. The strain rate in the gauge length for the four investigated alloys is given in Fig. 5. Thus the assumption of a constant strain rate cannot be made during the serrated flow. The inhomogeneity of strain resp. strain rate also implies that for each test where serrated flow occurs no uniform elongation can be measured as the process of elongation itself is inhomogeneous.

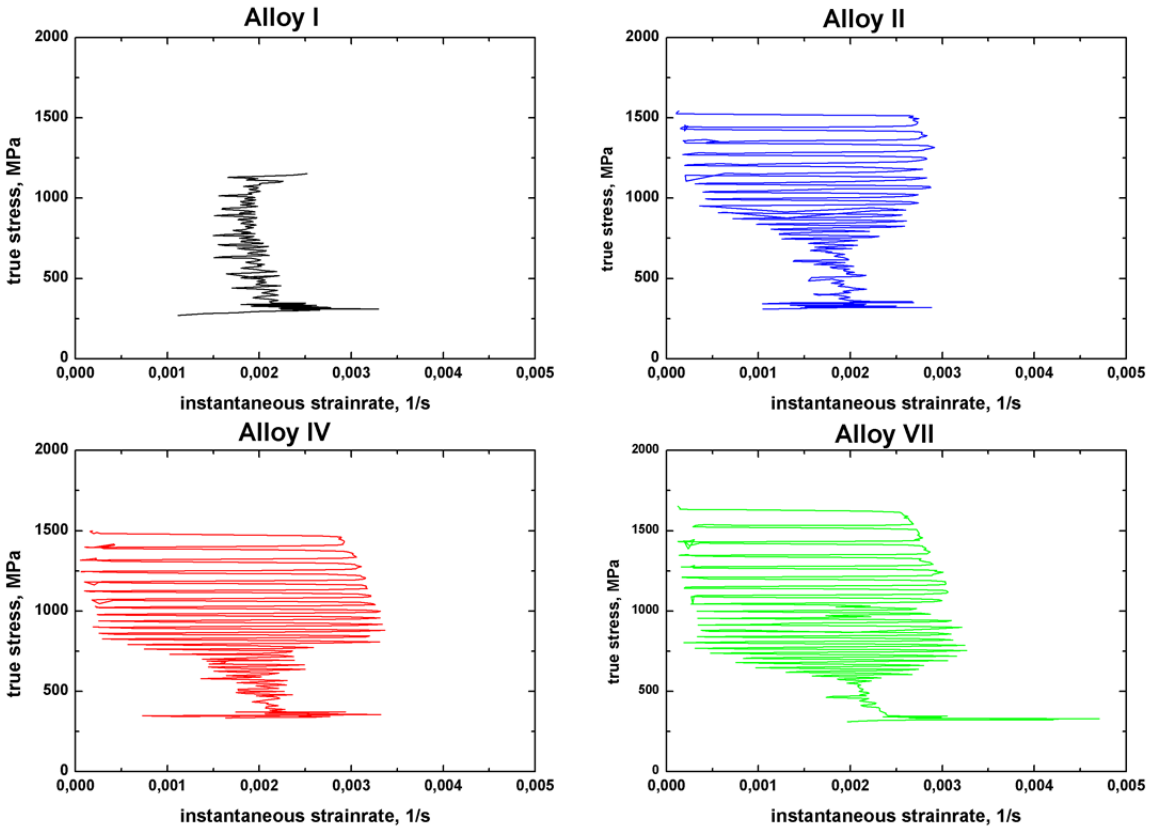

Figure 5: ISR vs. true stress-plot for the evaluation of localized plastic flow.

The next issue brought forward in the characterization of HMnS is the characterization of mechanical properties values. The standard assumes a homogenous distribution of strain and a homogenous elongation up to the onset of necking. As the high manganese steels show inhomogeneous deformation up to fracture this concept seems rather inappropriate. The plot of hardening and flow curve shows that the Considére-Criterion for necking is met in early stages of deformation without failure of the sample. On the other hand plotting a hardening curve calculated out of a fourth order polynomial fit of the flow curve to eliminate the serrations Considére-Criterion is not met, jet the sample has failed. On the other hand it can be seen that a stress overload for the start of a new deformation band leads to immediate fracture. This is either due to exhausted hardening capabilities on the site of localization, the joining of two deformation localizations that cannot be absorbed by the material or due to a preexisting damage (Fig. 6).

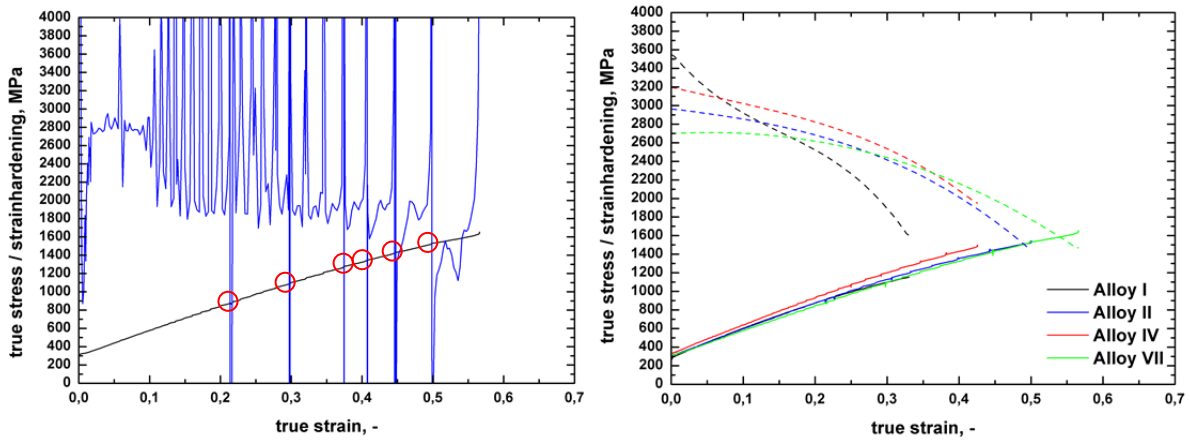

Figure 6: Left: Plot of flow curve and (unsmoothed) hardening curve of alloy VII. Considére-Criterion is matched at least 6 times (red circles) in the strain range from 0.2 to 0.5. Right: Plot of flow curve and smoothened hardening curve of the evaluated materials. Considére-Criterion is not matched for alloys I and II.

Conclusions: The inhomogenous deformation and hardening behavior of high manganese steels influences the mechanical testing to great extent. The assumptions valid for mild steels seem to be inappropriate for high manganese materials in case of strain homogeneity, strain rate, hardening, Considére-Criterion and temperature homogeneity. It can be proposed:

1. Localization of deformation in PLC-Bands leads to an inhomogeneous strain distribution and also inhomogeneity of thickness in the parallel length. Thus the concept of a uniform elongation is not applicable for these steels. The true stress has to be calculated at the smallest possible cross section of the specimen
2. The passage of PLC Bands leads to strain rate inhomogeneity on the gauge length, the global strain rate as well as the strain rate in each volume element jumps from very high to very low strain rates and vice versa. The assumption of a constant strain rate is not valid in this case.
3. Hardening can be described locally and globally. Global description of Hardening shows superior hardening behavior in comparison with AHSS
4. Considere Criterion is matched even in early stages of deformation when a PLC Band is formed, yet it does not lead to immediate fracture or local necking but to a stretching of the sample from the local necked area in direction of the lower deformation. Fracture occurs in some cases without the Considére-Criterion being met.

Acknowledgement: The authors gratefully acknowledge the financial support in the frame of Collaborative Research Center SFB 761 – “steel *ab initio*” by Deutsche Forschungsgemeinschaft (DFG). For their contribution to this work by supplying cold rolled material, the authors would like to express their special thanks to the project partners in the Department of Metal Forming (IBF) of RWTH Aachen University.

References

[1] C. Scott, S. Allain, M. Faral, N. Guelton: Revue de Métallurgie (2006), No. 6, pp. 293-302.

[2] A. Saeed-Akbari, J. Imlau, U. Prahl, W. Bleck: Metallurgical and Materials Transactions A 40A (2009), pp. 3076-3090.

[3] S. Allain, J.-P. Chateau, O. Bouaziz, S. Migot, N. Guelton: Materials Science and Engineering A 387-389 (2004), pp. 158-162.

[4] A. S. Hamada: Doctoral Thesis, ACTA Universitatis Ouluensis C281, Oulu, Finland, (2007)

[5] S. Allain: Doctoral Thesis, Institut Polytechnique de Loraine, (2002)

[6] S. Allain, P. Cugy, C. Scott, J.-P. Chateau, A. Rusinek, A. Deschamps Int. J. Mat. Res. (Formerly Z. Metallkd.) 99 (2008) 7, pp.734-737

[7] L. Chen, H.-S. Kim, S.-K. Kim, B.C. De Cooman, ISIJ International, Vol. 47 (2007), pp. 1804-1812.

[8] P.D. Zavattieri, V. Savic, L.G. Hector Jr. J.R. Fekete, W. Tong, Y. Xuan, International Journal of Plasticity 25 (2009), pp. 2298-2330

[9] J.-K. Kim, L. Chen, H.-K. Kim, S. K. Kim, Y. Estrin, B.C. De Cooman, Metallurgical and Materials Transactions A, 40A (2009), 3147-3158.

[10] A. Saeed-Akbari, Doctoral Thesis, Departement of Ferrous Metallurgy of RWTH Aachen University, 2011

[11] A. Wijler et al.: Acta Metall. 20(1972), 355.